



Contents lists available at ScienceDirect

Bioorganic & Medicinal Chemistry Letters

journal homepage: www.elsevier.com/locate/bmcl

Fragment-based discovery of potent ERK2 pyrrolopyrazine inhibitors

Daniel J. Burdick^{a,*}, Shumei Wang^a, Christopher Heise^b, Borlan Pan^c, Jake Drummond^b, JianPing Yin^c, Lauren Goeser^a, Steven Magnuson^a, Jeff Blaney^d, John Moffat^b, Weiru Wang^{c,*}, Huifen Chen^{d,*}

^a Department of Discovery Chemistry, Genentech, Inc., South San Francisco, CA 94080, United States

^b Department of Biochemical Pharmacology, Genentech, Inc., South San Francisco, CA 94080, United States

^c Department of Structural Biology, Genentech, Inc., South San Francisco, CA 94080, United States

^d Department of Computational Chemistry, Genentech, Inc., South San Francisco, CA 94080, United States

ARTICLE INFO

Article history:

Received 12 June 2015

Revised 7 August 2015

Accepted 14 August 2015

Available online xxx

Keywords:

ERK2

Pyrrolopyrazine

Fragment-based

Extracellular-regulated kinase

ABSTRACT

A fragment-based lead discovery approach was used to discover novel ERK2 inhibitors. The crystal structure of *N*-benzyl-9*H*-purin-6-amine **1** in complex with ERK2 elucidated its hinge-binding mode. In addition, the simultaneous binding of an imidazole molecule adjacent to **1** suggested a direction for fragment expansion. Structure-based core hopping applied to **1** led to 5*H*-pyrrolo[3,2-*b*]pyrazine (**3**) that afforded direct vectors to probe the pockets of interest while retaining the essential hinge binding elements. Utilizing the new vectors for SAR exploration, the new core **3** was quickly optimized to compound **39** resulting in a greater than 6600-fold improvement in potency.

© 2015 Elsevier Ltd. All rights reserved.

The Extracellular-regulated kinases ERK1/MAPK2 and ERK2/MAPK1 are the central effector nodes of the Ras/Raf/MEK pathway.¹ These kinases are responsible for transducing mitogenic and pro-survival signals from growth factor receptors as well as oncogenic mutant forms of Ras and Raf, and are therefore critical mediators of oncogenic signaling in a large proportion of cancers and tumor types. Downstream effects of ERK1/2 signaling relevant to cancer include activation of the mitogenic transcription program, regulation of protein synthesis through the Rsk kinases, and pro-survival signaling through the Bad/Bim pathway. The validity of the Ras/ERK pathway as a target for cancer therapeutics has been demonstrated with inhibitors of Raf and MEK kinases.² Since ERK1/2 are the sole catalytic substrates of MEK1/2, it is likely that small-molecule inhibitors of ERK would be equally as effective as MEK inhibitors while presenting opportunities for novel chemical matter and differential effects on pathway feedback and crosstalk.

In order to find novel ERK2 inhibitors, we screened a small fragment library using an NMR-based saturation transfer difference (STD) assay³ and using a surface plasmon resonance (SPR) assay.⁴ Herein we describe our efforts to improve the fragment hits obtained in the screen which led to the discovery of a novel and potent compound **39**.

The synthesis of compounds **7–21** and **22–39** was accomplished as outlined in Scheme 1. Commercially available boronic acids or their pinacol esters were coupled to 2-bromo-5*H*-pyrrolo[3,2-*b*]pyrazine **4** using standard Suzuki cross coupling methods to generate the C2 substituted analogues **7–21**.⁵ Treatment of the pyridine analogue **14** or the pyrazole analogue **17** with NIS in acetone cleanly provided the 7-iodo intermediates, which were then converted to compounds **40** and **41** by tosyl protection. These intermediates were subjected to standard Suzuki cross coupling methods with a number of different boronates followed by base promoted removal of the tosyl groups to generate analogues **22–39**.

We screened a small 635 member fragment library by using NMR-STD and SPR. The NMR-STD assay yielded 54 primary hits and the SPR assay resulted in 78 hits. Thirteen compounds overlapped in both the SPR and NMR screens. Subsequent SPR *K_D* measurements of these hits identified compounds **1** and **2** as the most ligand efficient hits (LE)⁶ (Fig. 1A).

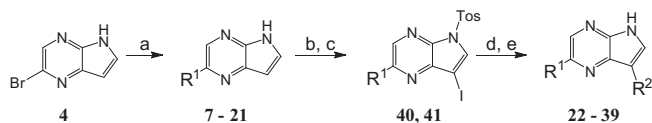
To elucidate the binding interactions of fragments **1** and **2** with ERK2 we determined their co-crystal structures with un-phosphorylated ERK2 protein. As illustrated in Figure 1B and C, compounds **1** and **2** bound in the ATP binding cleft and formed three hydrogen-bonds with the backbone of the hinge region comprising residues Asp106 though Met108. In addition, we observed some extra electron density in a pocket adjacent to the fragment, which was too large to be interpreted as a structural water. After reviewing the protein purification procedure, we interpreted this density as an imidazole molecule that had co-purified with the protein. Interest-

* Corresponding authors.

E-mail addresses: burdick.dan@gene.com (D.J. Burdick), wang.weiru@gene.com (W. Wang), chen.huifen@gene.com (H. Chen).

<http://dx.doi.org/10.1016/j.bmcl.2015.08.048>

0960-894X/© 2015 Elsevier Ltd. All rights reserved.



Scheme 1. (a) $[\text{PdCl}_2(\text{dppf})]\text{CH}_2\text{Cl}_2$, aryl-B(OH) $_2$ or pinacol ester, 1 M Na_2CO_3 , CH_3CN ; (b) NIS, acetone; (c) NaH, TosCl, DMF; (d) $[\text{PdCl}_2(\text{dppf})]\text{CH}_2\text{Cl}_2$, appropriate aryl-B(OH) $_2$ or pinacol ester, 1 M Na_2CO_3 , CH_3CN ; (e) 1 M NaOH, MeOH, THF.

ingly, the imidazole is within hydrogen-bond distance to the side chains of Asp111 and Lys114, indicative of the potential for engaging additional hydrogen bonds to the protein by linking the fragments (Fig. 1).

We then investigated whether fragment expansion into the imidazole-binding site can enhance the potency. Analysis of crystal structures (Fig. 1) indicated that although both compounds **1** and **2** form the hydrogen bond interactions with the hinge, the purine core of compound **1** is more co-planar with the imidazole ring. This co-planarity may allow substitutions at positions 2 and 6 of the purine core to reach the imidazole binding site. Compound **2** was deemed less interesting because it sits well above the plane of the imidazole ring and it was not obvious how to engage the imidazole binding pocket; thus we focused our attention on **1**.

Initial modification of the purine along the accessible vectors at C2 and C6 did not lead to a significant improvement in potency and ligand efficiency rapidly decreased (data not shown). It quickly became clear that an alternate ring system that provided access to different vectors was needed.

Alternative cores were considered that would maintain a two or three point hinge interactions like the initial fragment **1**; reach the back pocket to form additional hydrogen bond interactions; and make an additional contact in the imidazole fragment region. An additional consideration to move away from the heavily explored purine scaffold, is that purines are the basis of many drug discovery campaigns and finding novel inhibitors may prove to be difficult.⁷

After determining the key pharmacophore features and considering a number of different cores, we proposed changing the purine core of the screening hit to 5H-pyrrolo[3,2-*b*]pyrazine (**3**, Fig. 2). This core is less represented in the literature relative to the purine.⁸ Furthermore this scaffold retains the same hydrogen bonding donor/acceptor pair available for interacting with the hinge of the protein and it has the proper pK_a range at N7 to ensure that it acts as a hydrogen bond acceptor. In addition, this core has carbon atoms at the proper positions to furnish vectors that point toward the back side of ATP binding pocket as well as the region where the imidazole was observed in the crystal structure.

The un-substituted 5H-pyrrolo[3,2-*b*]pyrazine core **3** was evaluated by SPR and was found to be slightly less active than the frag-

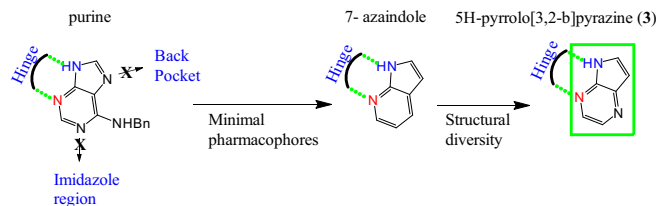


Figure 2. Proposed core hopping strategy: replacement of the purine with the minimal pharmacophore 7-azaindole would provide the needed hinge hydrogen bonding interactions as well as providing new vectors to probe the imidazole region and the back pocket.

ment hit **1** (Table 1); however, it is approximately twice as ligand efficient. We determined the crystal structure of **3** bound to ERK2 to confirm the binding mode. As shown in Figure 3, compound **3** engages the hinge through both classical and C–H type hydrogen bonds with Asp106 and Met108, and again indicated that substitution at C2 and C7 can potentially generate additional interactions with Asp111, Lys114 and Gln105. Encouraged by these results, we tested a small series of commercially available 5H-pyrrolo[3,2-*b*]pyrazines in the SPR assay. A bromine at C2 of the 5H-pyrrolo[3,2-*b*]pyrazine core was tolerated (**4**) while halide substitution at C7 (**5** and **6**) improved potency and preserved good ligand efficiency. These initial results gave us confidence that we could expand SAR along these vectors and we embarked on a medicinal chemistry campaign to further improve the 5H-pyrrolo[3,2-*b*]pyrazine series.

We then explored different groups at the 2 position of pyrrolo[3,2-*b*]pyrazine (Table 2). Addition of a phenyl group (**7**) increased the activity by more than 4 fold (Table 2), whereas a bromo group (**4**) at this position showed no appreciable change in binding affinity (Table 2).

These results suggested aryl substitutions would be productive at the C2 position. To further explore the C2 position, we made a series of analogues substituted with aryl and small heteroaryl rings to mimic the imidazole that we observed in the initial crystal structures. Analysis of the aryl analogues tested revealed that meta substitutions (**8** and **9**) were not tolerated most likely due to steric clashes with Glu109 and Asp111. *para* substitutions (**10** and **11**) showed marginal improvement over the phenyl analogue regardless of the electronic nature of the functional group. The 4-fluoro (**12**) and 4-hydroxy compounds (**13**) were the most potent of this set of phenyl analogues, which indicated that a small hydrogen bond accepting group may be advantageous and would interact with Lys114. The pyridyl analogues, which contain a hydrogen bond acceptor in the ring, were also active. The *para*-pyridyl (**14**) and 2-fluoropyridin-4-yl (**15**) analogues were more active and had higher ligand efficiencies than the *meta* analogue (**16**) possibly

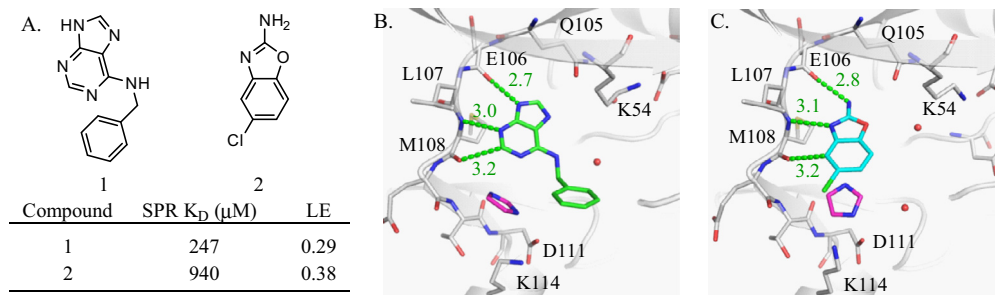
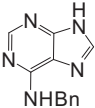
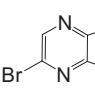


Figure 1. (A) Structure and activity of two potent and ligand efficient fragments found in both the NMR STD and SPR screens. (B) Crystal structure of *N*-benzyl-9H-purin-6-amine (**1**) (PDB ID: 4QP1) and (C) 5-chlorobenzo[d]oxazol-2-amine (**2**) (PDB ID: 4QP2) in complex with ERK2. Both fragments form multiple hydrogen bonds (including non-classical C–H type) with the kinase hinge as shown by green dashed lines (distances are in angstroms). The crystallographic imidazole fragments are colored in magenta.

Table 1
Activities of fragment screening hit **1** and initial core vector analogues

Compound	Structure	SPR K_D (μ M)	LE
1		247	0.29
3		343	0.53
4		319	0.48
5		97	0.55
6		125	0.49

due to better hydrogen bonding with Lys114. Heterocycles that present a hydrogen bond donor/acceptor combination were also well tolerated (**17–21**). Compound **17** had the best potency and ligand efficiency and is greater than 30 fold more potent than the parent 2-bromo analogue (**4**). Pyrazole **17** displays both a hydrogen bond donor and acceptor and was 4-fold more potent than the matched pair compound **18**, which has the hydrogen bond donor masked by a methyl group. Compound **17** was the most potent and ligand efficient analogue of this series and it is apparent in the co-crystal structure (Fig. 3) that the pyrazole makes favorable hydrogen bond and polar interactions with both Asp111 and Lys114 and occupies the space where the crystallographic imidazole was observed. The methyl substituted analogues (**19** and **20**) were less potent than the un-substituted pyrazole even though they contain the same hydrogen bond donor and acceptor as **17**. The reduction in potency can be attributed to less optimal dihedral angles imposed by the methyl groups. Indazole **21** was five times less potent than the pyrazole **17** presumably because it extends beyond the interactions of Asp111 and Lys114.

Having established two favorable C2 moieties, 4-pyridyl and 4-pyrazole, we turned our attention to substitutions at C7 of the

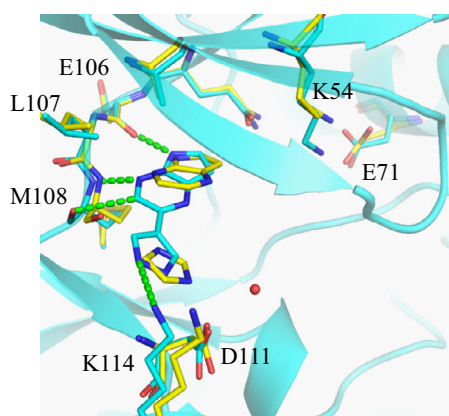


Figure 3. Crystal structure of compound **3** in complex with ERK2 (yellow, PDB ID: 4QP6) overlaid with the structure of compound **17** in complex with ERK2 (cyan, PDB ID: 4QP7). Intermolecular hydrogen bonds (including non-classical C–H type) between **17** and ERK2 are shown in green dashed lines.

pyrrolo[3,2-*b*]pyridine. Molecular modeling of potential inhibitors in the binding pocket of the protein indicated that a 3-pyridyl or 5-pyrimidyl moiety at the 7 position of the pyrrolo[3,2-*b*]pyridine core should place the ring nitrogen within hydrogen bonding distance of the gatekeeper residue Gln103. Compounds **22** and **23** (Table 3) were, respectively, 29-fold and 5.3-fold more potent than the pyridyl analogue **14**. In a similar fashion, compounds **24** and **25** were 21-fold and 5.6-fold more potent than compound **17**. Based on the activity of compound **22**, a series of substituted 3-pyridyl and pyrazole analogues were made at C7 and their activities were compared to compound **22**. Small electron donating groups in the 4 position of the 3-pyridyl moiety (**26–28**) were approximately equipotent to the parent pyridyl (**22**). Introduction of an electron-withdrawing group (**29**) increased potency over 2-fold presumably due to the change in pK_a of the pyridyl nitrogen making it a better hydrogen bond acceptor and the introduction of a van der Waals interaction between the chlorine and Tyr 36.

The crystal structure of **24** in ERK2 (Fig. 4A) confirmed our modeling hypothesis. The pyrrolo[3,2-*b*]pyridine core and pyrazole binds to the hinge and front pocket like compound **17** and the 3-pyridyl indeed binds to the back pocket with the pyridyl nitrogen forming a hydrogen bond to the catalytic Lys54. In addition, a water molecule is also within hydrogen bond distance of the pyridyl nitrogen, which may offer additional potency improvement. There is also a notable difference in the location and orientation of Tyr36 in the P-loop. Tyr36, which packs against the alpha C helix in the crystal structure of **24** (Fig. 4A) has been pulled in with its aromatic ring slightly stacking over the 3-pyridyl moiety. The C6 position of the pyridine is 3.6 and 4.3 angstroms away from atoms in Tyr36 and Asp167, respectively, and thus limits the size of functional groups that can be tolerated in this region. The structure also revealed that some space is available towards the sugar and alpha phosphate binding region.

Replacement of the 3-pyridyl group at C7 (**22**) with a 5-pyrazole moiety (**30**) decreased inhibitor activity two fold whereas a slight increase was obtained when the 3-pyridyl was replaced with a 4-pyrazole group (**31**). The potency decrease of **30** could be a result of a less optimal hydrogen bond between the pyrazole N2 and Lys54 due to tautomerization. In compound **31**, on the other hand, the pyrazole is symmetric and would present a hydrogen bond acceptor proximal to Lys54 regardless of tautomerization. In addition, we could substitute at the NH of the 4-pyrazole to not only

Table 2
SAR of position 2 of 5H-pyrrolo[3,2-*b*]pyridines

Compound	R ¹	IC ₅₀ active ERK (μ M)	LE
4	Br	>200	<0.50
7	Ph	50.1	0.39
8	3-Benzamide	>200	<0.28
9	3-Hydroxyphenyl	>200	<0.32
10	4-Benzamide	44.1	0.33
11	4-Methoxyphenyl	89.7	0.32
12	4-Fluorophenyl	29.7	0.39
13	4-Hydroxyphenyl	12.4	0.42
14	4-Pyridyl	11.7	0.45
15	2-Fluoropyridin-4-yl	21.6	0.40
16	3-Pyridyl	71.5	0.38
17	4-Pyrazole	5.9	0.51
18	<i>N</i> -Me-4-pyrazole	22.5	0.43
19	3,5-Dimethyl-4-pyrazole	14	0.41
20	3-Methyl-4-pyrazole	22.2	0.43
21	6-Indazole	31.9	0.34

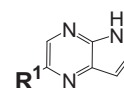
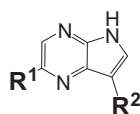


Table 3
Structure activity relationship of C2 4-pyridyl analogues

Compound	R ¹	R ²	IC ₅₀ active ERK (μM)	LE
14	4-Pyridyl	H	11.7	0.45
22	4-Pyridyl	3-Pyridyl	0.407	0.42
23	4-Pyridyl	5-Pyrimidyl	2.2	0.37
17	4-Pyrazole	H	5.9	0.51
24	4-Pyrazole	3-Pyridyl	0.28	0.45
25	4-Pyrazole	5-Pyrimidyl	1.05	0.41
26	4-Pyridyl	6-Methoxypyridin-3-yl	0.252	0.43
27	4-Pyridyl	6-Aminopyridin-3-yl	0.468	0.45
28	4-Pyridyl	6-Methylpyridin-3-yl	0.634	0.41
29	4-Pyridyl	6-Chloropyridin-3-yl	0.182	0.42
30	4-Pyridyl	5-Pyrazole	0.94	0.41
31	4-Pyridyl	4-Pyrazole	0.354	0.44

reduce the desolvation penalty but also introduce additional interactions towards the sugar phosphate binding region. Simple methyl alkylation (**32**) of the nitrogen resulted in a potency increase and not a decrease; this suggests that the NH of the pyrrole is not making any particular interaction with the protein (Table 4). Ethylation of the pyrazole (**33**) led to a two-fold improvement in potency compared to compound **31** and extending to a propyl (**34**) resulted in another doubling of potency.

A crystal structure of **34** in ERK2 (Fig. 4B) was determined and as expected the pyrrolopyrazine core binds to the kinase hinge with the 4-pyridyl ring at C2 facing solvent and the C7 4-pyrazole binding in the back pocket. The N2 acceptor atom of the 4-pyrazole is 4.5 Å from the Lys54 tertiary amine and is likely interacting with Lys54 through a water-mediated hydrogen bond (the water is not resolved) while the propyl on N1 binds in a polar region near the sugar phosphate group of ATP. Similar to the crystal structure of **24** (Fig. 4A), Tyr36 of the P-loop adopts the same conformation and forms close hydrophobic interactions with the N1-propyl tail (**34**). In an attempt to induce a Tyr36-out conformation, which would give more room for expansion, we decided to pursue a few larger substitutions. The 2-isobutyl substituted analog (**35**) was slightly less potent than **31**. The hydroxyl propyl (**36**) analog did not improve potency, but on the contrary led to a potency drop of 9-fold, possibly due to desolvation penalties. The morpholine ethyl substitution (**37**) was not well tolerated and led to 6-fold potency drop compared to compound **31**. A phenethyl substitution (**38**) proved to be very detrimental, resulting in a 2 μM IC₅₀.

However, to our great satisfaction, the benzyl substitution (**39**) resulted in a 10-fold increase in potency compared to compound **31**. Compound **39** was the first of the pyrrolopyrazine series reaching below 50 nM potency in the ERK2 biochemical assay, and represents an excellent starting point for further optimization. A crystal structure of **39** in complex with ERK2 was determined and indeed the P-loop adopts a Tyr36-out conformation (Fig. 4C). Tyrosine 36 in this structure has swung out to open up more space under the P-loop such that the phenyl ring in **39** binds where the Tyr36 ring occupied in the pulled in conformation (Fig. 4A and B). The flexibility of the P-loop will allow further optimization of the benzyl moiety to improve potency and other properties of this promising molecule.

Purine inhibitor (**1**) was discovered in a NMR-STD and SPR fragment screen. X-ray crystallography of early fragments revealed an unexpected imidazole molecule in the vicinity of the kinase hinge. Exploitation of the imidazole and back pocket of the binding site could not be achieved with the initial purine scaffold. Core hopping to a 5H-pyrrolo[3,2-*b*]pyrazine core provided efficient vectors to reach both the imidazole region and the back pocket while keeping the correct donor and acceptor atoms to form hydrogen bonds with the hinge. Beneficial interactions were formed with Lys114 and possibly Asp111 in the front pocket with either a 4-pyridyl or 4-pyrazole substitution on the 5H-pyrrolo[3,2-*b*]pyrazine core at C2. Further substitutions at C7 showed that a hydrogen bond could be formed with Lys54 and Tyr36 could be moved into a position under the P-loop giving a greater enhancement in potency.

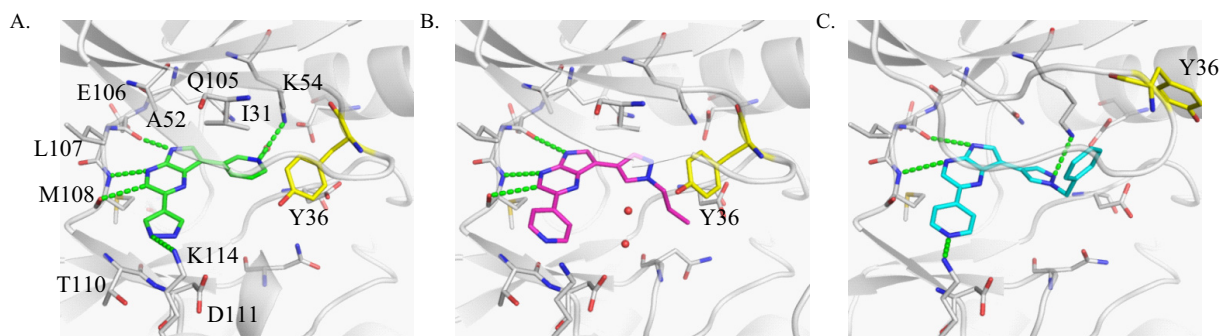
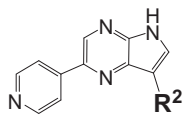


Figure 4. (A) Crystal structure of compound **24** (green) in complex with ERK2 (PDB ID: 4QP8). (B) Crystal structure of compound **34** (magenta) in complex with ERK2 (PDB ID: 4QP9). (C) Crystal structure of compound **39** (cyan) in complex with ERK2 (PDB ID: 4QPA). Tyr36 in P-loop is colored in yellow. Intermolecular hydrogen bonds between compounds and ERK2 are shown in green dashed lines.

Table 4

The effect of substitution on 7-(1*H*-pyrazol-4-yl)-2-(pyridin-4-yl)-5*H*-pyrrolo[2,3-*b*]pyrazine analogues



Compound	R ²	IC ₅₀ ERK2 LC3K (μM)	LE
31		0.354	0.44
32		0.072 ^a	0.47
33		0.149	0.43
34		0.071	0.43
35		0.091	0.41
36		0.623	0.36
37		0.416	0.31
38		2.0	0.18
39		0.037	0.38

^a Value in the OMNIA ERK2 assay. Values for compounds have the same rank order.

Ultimately, a greater than 6600-fold increase in potency and an increase in ligand efficiency were achieved after moving from purine **1** to compound **39**. Compound **39** became the starting point for

further optimization and the results of this effort will be disclosed in a subsequent Letter.

Acknowledgments

We thank the Analytical, Biopharmacology, Compound Management, NMR, Pharmacokinetics, and Structural Biology colleagues for their contributions. Crystallographic data were collected at the Advanced Light Source (ALS). ALS is supported by the Director, Office of Science, Office of Basic Energy Sciences, of the U.S. Department of Energy under Contract No. DE-AC02-05CH11231.

Supplementary data

Supplementary data (synthetic procedures, assay protocols and crystallographic refinement statistics) associated with this article can be found, in the online version, at <http://dx.doi.org/10.1016/j.bmcl.2015.08.048>.

References and notes

- Wong, K. K. *Recent Pat. Anticancer Drug Discov.* **2009**, *4*, 28.
- Montagut, C.; Settleman, J. *Cancer Lett. (Shannon, Ireland)* **2009**, *283*, 125.
- Mayer, M.; Meyer, B. J. *Am. Chem. Soc.* **2001**, *123*, 6108.
- Erlanson, D. A. In *Fragment-based Drug Discovery and X-ray Crystallography: Topics in Current Chemistry*; Springer: Berlin, Germany, 2011; Vol. 317, p 1.
- Suzuki, A. J. *Organomet. Chem.* **2002**, *653*, 83.
- (a) Hopkins, A. L.; Groom, C. R.; Alex, A. *Drug Discovery Today* **2004**, *9*, 430; (b) Abad-Zapatero, C. *Expert Opin. Drug Discov.* **2007**, *2*, 469.
- (a) Song, Y.; Xu, Q.; Bauer, S. M.; Jia, Z. J.; Mehrotra, M.; Pandey, A. *PCT Int. Appl.* **2009**, WO 2009131687 A2.; (b) Huang, W.; Zhu, X.; Wang, Y.; Azam, M.; Wen, D.; Sundaramoorthi, R.; Thomas, M. R.; Liu, S., et al. *J. Med. Chem.* **2009**, *52*, 4743; c Green, S.; Frame, S.; Fleming, I. *PCT Int. Appl.* **2008**, WO 2008122779 A1.; (d) Hauser, D. R. J.; Scior, T.; Domeyer, D. M.; Kammerer, B.; Laufer, S. A. *J. Med. Chem.* **2007**, *50*, 2060.
- (a) Gelbard, H. A.; Dewhurst, S.; Goodfellow, V. S.; Wiemann, T. *PCT Int. Appl.* **2010**, WO 2010068483 A2.; (b) Graczyk, P.; Bhatia, G. S. *PCT Int. Appl.* **2010**, WO 2010015803 A1.; (c) Dubois, D. J.; Elworthy, T. R.; Hendricks, R. T.; Hermann, J. C.; Kondru, R. K.; Lou, Y.; Owens, T. D.; Smith, D. B. *U.S. Pat. Appl. Publ.* **2009**, US 20090215785 A1.; (d) Arnold, W. D.; Bonnaud, P.; Chen, C.; Eastman, B.; Gosberg, A.; Grادل, S. N.; Hopkins, S.; Li, Z.; McDonald, I.; Sprengeler, P. A.; et al. *PCT Int. Appl.* **2008**, WO 2008124850 A1.